Crystalline deposits reveal caste identity of late embryos and larvae of the ant *Cardiocondyla obscurior*

Tobias Wallner[1]

Eva Schultner[1]

Jan Oettler[1*]

[1]Zoology/Evolutionary Biology, University of Regensburg, Universitätsstrasse 31, 93053 Regensburg, Germany

*corresponding author

ORCID:

Tobias Wallner: 0000-0001-9135-6456

Eva Schultner: 0000-0002-5069-9732

Jan Oettler: 0000-0002-8539-6029

Keywords:

Caste; social insects, ant larvae; urate; ovarian development; eco-evo-devo

Abstract

Social insects are interesting models for the study of anticipatory developmental plasticity because of the striking differentiation into reproductive queens and functionally sterile workers. A few ant genera, including *Cardiocondyla*, represent the pinnacle of social evolution in the Hymenoptera, where workers have completely lost their reproductive organs, minimizing reproductive conflicts between queens and workers. Here we show that late embryos and larvae of queens of the ant *C. obscurior* can be identified by the appearance of urate deposits around the forming ovaries. The discovery of caste-specific urate patterns in *C. obscurior* and three additional *Cardiocondyla* species will facilitate future studies of developmental plasticity in ants.

Introduction

Alternative developmental trajectories leading to the division of labour between reproductive queens and non-reproductive workers form the basis of superorganismality, thereby permitting one of the major transitions in evolution [1]. Research on caste development in ants has a long tradition (e.g. [2-5], and conceptual discussions are ongoing (e.g. [6,7]. However, how the processes of caste determination and differentiation are regulated at a proximate level is not well understood.

Compared to honeybees, where caste fate is under strict nutritional control, the factors underlying caste fate in ants are more diverse, ranging from genetic to socio-environmental [8]. With this comes variation in the timing of developmental divergence (e.g. [4,9], so that ants exhibit different degrees of "reproductive constraints" [9]. In some species of Ponerine ants, workers retain full reproductive potential, including the ability to mate and store sperm. In the majority of ant species workers have lost the spermatheca but retain more or less functional ovaries capable of producing haploid, male-destined eggs. Finally, workers from 11 genera completely lack ovaries. These obligately sterile workers are an example of an extended phenotype without any direct fitness, representing a highly derived form of superorganismality. The biology of some myrmicine species with fully sterile workers has been studied extensively (*Cardiocondyla obscurior*, *Monomorium pharaonis*, *Pheidole* spec., *Solenopsis invicta*), but comparably little is known about their development. Even less is known about development in the remaining seven genera with workers lacking reproductive organs (to the best of our knowledge; Myrmicinae: *Wasmannia*, *Tetramorium*, *Pheidologetum*; Dorylinae: *Eciton*; Ponerinae: *Leptogenys*, *Hypoponera*, *Anochetus*).

Across the range of reproductive constraints, a diverse set of signals spanning nature and nurture is likely to be involved in caste-specific development. Together with the facts that ant larval mobility is variable, ant brood is reared in piles, and brood is often

relocated and can serve functional roles in the colony [10], this has rendered the study of ant development a more complex problem compared to *Drosophila* research. In particular, it has been difficult to study caste-specific developmental trajectories because it is not possible to distinguish worker-destined larvae from queen-destined and male-destined larvae (e.g. [11]. Here, we close this gap for the ant *Cardiocondyla obscurior* by showing that queen- and worker-destined embryos and larvae can be visually distinguished by crystalline deposits surrounding the developing ovaries of queen-destined larvae. This discovery will facilitate the study of caste determination and differentiation at the extreme end of the superorganismality spectrum, thus bringing us closer to a general understanding of the mechanisms facilitating the evolution of social insects.

Methods

Ants

C. obscurior is a cosmotropical tramp ant [12], with a very streamlined genome (~193MB, [13]), the smallest ant genome known to date. Adult queens and workers differ in size and morphology and workers lack ovaries. Larvae develop via three larval instars which can be distinguished by the shape of the body and the degree of sclerotization of the mandibles [14]. The ants used in this study were all from the Old World lineage [13], maintained in the lab since 2010. Stock colonies were kept in a climate chamber under a 12h/12h and 22°C/26°C night/day cycle at 70% humidity. Experimental colonies were kept in round plaster-bottom nests with nest indentations covered by dark foil under the same conditions. All colonies were provided with water and fed three times a week with honey and pieces of cockroaches and fruit flies.

White crystalline spots

All larvae of *C. obscurior* exhibit white spots. After producing semi-thin sections (see below), we used a polarization filter that revealed a crystalline reflection. These crystalline structures are common in insect larvae and have been described as urate crystals (see discussion). Hence, because it is a parsimonious explanation we use "urate deposits" in the following when we refer to the white spots, even though we are aware that this may not be correct and requires future verification.

Urate deposit localization

We characterized urate deposits in eggs and first instar (L1), second instar (L2) and third instar (L3) larvae as unpaired (= worker-destined) or paired (= queen-destined) by visually inspecting brood from stock colonies under a stereomicroscope. For better detection of the patterns, eggs and L1 larvae were submerged in a dissection dish containing PBT (0.3 %), after which they were mounted on a microscope slide and sealed with nail polish. From each development stage, we selected and photographed one representative individual with a paired pattern and one individual with an unpaired pattern using a stereomicroscope connected to a camera (Keyence VHX 500FD, Neu-Isenburg, Germany).

We additionally characterized urate patterns of third instar larvae from seven *Cardiocondyla* species available in the lab. We further examined brood of six species from four subfamilies available as live colonies. Lastly, we accessed Alex Wild's photo library for a broader overview of species (https://www.alexanderwild.com/Ants/Natural-History/Metamorphosis-Ant-Brood/).

Caste fate and survival according to urate deposits

We tracked development of all stages to confirm that urate localization patterns are associated with caste in *C. obscurior*. Brood was sampled from several stock colonies and sorted by development stage and urate pattern as described above. Eggs and L1

111 larvae were transferred to filter paper to remove excessive buffer. Eggs were then
112 transferred in groups of ~15 to experimental colonies containing 10 workers (eggs:
113 paired=192, unpaired=165). L1 larvae were transferred to experimental colonies
114 containing 10 workers; two colonies were setup with 17 queen-destined larvae each,
115 and two colonies with 19 and 4 for worker-destined larvae, respectively (L1:
116 paired=34, unpaired=23). L2 and L3 larvae were transferred in groups of ten to
117 experimental colonies containing 10-12 workers (L2: paired=50, unpaired=40, L3:
118 paired=50, unpaired=40). Experimental colonies were monitored three times per
119 week and, when necessary, workers added from the corresponding stock colonies to
120 standardize worker number. All pupae were counted and classified according to
121 female caste until no more brood remained. From these data, we calculated average
122 survival until pupation and caste ratios. Survival of castes and accuracy of caste
123 prediction were tested with Fisher exact tests (fisher.test in R).

124 We tracked development of L3 larvae from six additional *Cardiocondyla* species, *C.*
125 *wroughtonii*, *C. argyrotricha*, *C. thoracica*, *C. minutior*, *C. nuda*, *C. venustula*,
126 spanning the phylogeny with exception of the palearctic clade [15], to validate that
127 urate deposit patterns accurately predict caste.

128

129 Larval histology

130 L3 larvae were collected from stock colonies of *C. obscurior* and sorted according to
131 their urate patterns. Sorted larvae were transferred into a fixation solution consisting
132 of 25% glutaraldehyde (GAH) in cacodylate buffer [(50 mM cacodylic acid, pH 7.3)
133 containing 150 mM Sucrose] (GAH : cacodylate buffer = 1 : 12,5) and kept overnight
134 at 11 °C. Samples were then rinsed in cacodylate buffer on ice, and fixated in 4%
135 osmium tetroxide in cacodylate buffer. After fixation, larvae were washed in
136 cacodylate buffer, dehydrated in a graded ethanol series and embedded in Epon.
137 Transversal semithin sections of 1 µm were cut and stained with methylene blue and

138 Azur II (Richardson's stain). Semi-thin sections were scanned with a Zeiss Primo Star
139 microscope and imaged with a Moticam 580 digital microscope camera.

140

141 Ovary development

142 *C. obscurior* queen L2 and L3 larvae were dissected in PBT 0.3% (PBS 1x + Triton
143 0.3%) by cutting below the midgut with a micro scissor. The posterior part of the larvae
144 was cleared of excess fat tissue. The larval ovaries were placed in an ice-cooled well
145 filled with PBT. We chose two different stages of queen pupae based on their
146 development. Early-stage pupae were identified as unsclerotized white pupae with
147 unpigmented ommatidia and ocelli. Mid-stage pupae exhibit pigmented ommatidia
148 and ocelli. Ovaries from queen pupae and adults were obtained by carefully pulling
149 on the last tergite of the abdomen with forceps, which removes the entire
150 reproductive apparatus. Larval, pupal and adult ovaries were fixated in 4%
151 paraformaldehyde diluted in PBS for 20 min at room temperature. The fixated ovaries
152 were then washed three times with PBT for 15 min on a tumbler. After washing, the
153 ovaries were processed for staining.

154 Vasa protein was stained with a rat anti-vasa antibody and actin filaments were
155 visualized using a rabbit anti-actin antibody. Both antibodies were generated from
156 *Drosophila* [9]. Cell nuclei were stained using DAPI. The primary antibodies were
157 diluted 1:200 in PBT 0.3% with 5% normal goat serum overnight at room temperature
158 on a tumbler. To remove the primary antibody, the larval and pupal ovaries were
159 washed three times with PBT for 15 min. The secondary antibodies goat anti-rat and
160 goat anti-rabbit were used to visualize the rat anti-vasa and rabbit anti-actin
161 antibodies, both diluted 1:200 in PBT. After 2 h of incubation at room temperature,
162 the ovaries were again washed three times with PBT for 15 min each. Finally, the larval,
163 pupal and adult ovaries were washed with PBT containing DAPI (1:10000). Ovaries
164 were then mounted in Vectashield on a microscope slide and sealed with nail polish.

165 Images for the antibody staining were obtained using a Leica SP8 confocal
166 microscope under 40x and 63x objective lenses. Complete confocal series of ovarioles
167 of early- and mid-staged queen pupae were processed using the FIJI plugin TrakEM2
168 [16] for 3D rendering and analysis.

169 *Nanos* and *vasa* expression was measured in queens and workers from all larval
170 stages. L1 and L2 larvae were collected and transferred to individual 1.5 ml tubes (L1:
171 n=5 queen larvae, n=7 worker larvae; L2: n=5 queen larvae, n=5 worker larvae). L3
172 larvae were cut beneath the midgut at the posterior end (containing the developing
173 ovaries in queen larvae) and transferred to individual tubes (L3: n=5 queen larvae, n=4
174 worker larvae). All samples were immediately frozen in liquid nitrogen and stored at -
175 75°C prior to RNA extraction. Total RNA was extracted using the ReliaPrep RNA Cell
176 Miniprep Kit (Promega) and RNA concentrations measured using the Qubit RNA HS
177 Assay Kit (Invitrogen). RNA concentrations were standardized to 2.5 ng and RNA
178 reverse-transcribed to cDNA using the iScript gDNA Clear cDNA Synthesis Kit (Bio-
179 Rad Laboratories). Expression of the gene *nanos* was quantified with qPCR with the
180 primer pair nos_for/nos_rev and normalized with two housekeeping genes
181 (Y45F10D_JO1_for/Y45F10D_JO1_rev [17]) and Actin_JO1_for/Actin_JO1_rev; see
182 Table S1 for primer sequences). All qPCR reactions were performed in triplicates and
183 specificity of reactions confirmed with manual melt curve inspection. Relative target
184 gene expression was calculated as $2^{-\Delta Cq}$ following [18], using the geometric mean of
185 the two housekeeping genes for normalization.

186

187 Results

188 Queen and worker-destined eggs and larvae of *C. obscurior* can be distinguished, by
189 what appear to be urate crystals. In late embryos (Figure 1) and the three larval stages
190 (Figure 2, Figure S1), urate deposit patterns associated with queen caste are visible.
191 Queen patterns appear either as a string of pearls or are snail shell-like (Figure S2).

192 Handling L1 larvae results in high mortality, but L2 and L3 individuals can be attributed
193 to the two castes with high precision (Table 1).

194 Transversal semithin sections of L3 larvae revealed that worker larvae lack ovaries and
195 have urate deposits which are distributed randomly throughout the caudal end (Figure
196 3 A). These cluster in small aggregates (10-20 µm diameter) in proximity to
197 trophocytes (Figure 3 C, E). In queen larvae, urate crystals form voluminous
198 aggregations surrounding the developing ovaries, which contain several dozens of
199 developing oocytes (Figure 3 B, D, F). In both castes urate comes in the shape of
200 translucent birefringent spherocrystals.

201 Urate deposit patterns allowed for selection of queen-destined L2 and L3 larvae,
202 making it efficient to reconstruct ovarian development. In L2 larvae the developing
203 ovaries are visible as a bilateral cluster of germ cells located at the posterior end of
204 the last abdominal segments (Figure 4 A-D). The ovaries are in close proximity to the
205 caudal end of the central nervous system (Figure 4 D, CNS). The cluster of cells in L2
206 larvae then differentiate into three ovarioles per ovary in L3 larvae (Figure 4 E-H), with
207 the tips extending in an anterior-apical orientation (Figure S8). Disc-shaped cells can
208 be found which stack in a medial-lateral orientation (Figure 4 H, asterisk). These cells
209 are likely cap cells [19], which separate the germarium from the terminal filament [20].

210 In pupae, the ovaries are completely differentiated, with fully extended terminal
211 filaments (Figure 4 I-L). The germ cells in the germarium have differentiated into
212 cystocytes, which will later give rise to the oocyte with the associated nurse cells
213 (Figure 4 L) [21]. After reaching the adult stage, the fully matured ovarioles have egg
214 chambers, containing oocytes with their corresponding nurse cells (Figure 4 M-P). The
215 oocytes are surrounded by follicle cells, and these egg chambers are in different
216 stages of maturation (Figure 4 P). Reconstruction of the cystocytes inside the ovarioles
217 of early- and mid-staged queen pupae showed that the developing cells increase
218 significantly in size during pupation (Linear regression, R^2=0.9036, $p<0.001$) and that
219 cell size is highly variable (Figure S3).

220 The expression of the germline marker *nanos* was higher in L2 and L3 queen larvae
221 compared to worker larvae (Figure S4, L2: Mann-Whitney-U-test: W=24, p=0.016; L3:
222 W=20, p=0.016, Figure S4), but not in L1 larvae (W=25, p=0.27). *nanos* expression
223 increased over the course of development in queens, matching the developmental
224 state of the ovaries. The variation in *nanos* expression is conspicuously high in L2
225 queen larvae. In contrast, *vasa* expression was significantly higher in L1 (W=33,
226 p=0.010) and L3 queen larvae (W=20, p=0.016), but not in L2 larvae (W=17, p=0.421),
227 confirming that sampling based on urate patterns was successful, despite failure to
228 show this for L1 larvae in rearing experiments.

229 We found queen-like urate patterns in larvae of three additional *Cardiocondyla*
230 species (*C. venustula*, *C. wroughtonii* and *C. nuda*) (Figure S5, Table S2). In the
231 remaining four species (*C. thoracica*, *C. elegans*, *C. argyrotricha* and *C. minutior*) we
232 did not find obvious caste-specific patterns (Figure S6, Table S2).

233 39 of 41 additional species representing 30 genera from seven ant subfamilies had
234 larvae with obvious urate deposits (Table S3; Figure S7), but no species exhibited
235 paired urate deposits resembling the pattern observed in *Cardiocondyla* queen
236 larvae.

237

238 Discussion

239 "Auch ein blindes Huhn findet mal ein Korn" (German saying)

240 *Cardiocondyla* is unique among the Formicidae due to the evolution of wingless
241 fighter males and the repeated loss of the winged male morph across the genus [15].
242 Because colonies of *C. obscurior* can be easily reared and manipulated, the species
243 has been used to address questions in diverse biological contexts [22,23], ranging
244 from genome evolution [13,24], to social behavior [25], aging [26,27], symbiosis
245 [28,29], and phenotypic plasticity [17,30,31]. In this respect, *C. obscurior* has been
246 considered a "gold mine" (E. Abouheif pers. com.). Now, as is often the case in

247 mining, sheer luck has led to the discovery that queen and worker embryos and larvae
248 in some *Cardiocondyla* species can be distinguished using the localization of urate
249 deposits. We could not find a similar pattern in other ant genera, but 39 species from
250 30 genera is by far not representative of the vast diversity of ants. We hope that our
251 discovery inspires others to take a closer look at the brood of their favorite species.

252 In insects, urate is typically deposited in specialized cells – so-called urocytes [32] –
253 which together with trophocytes [32] and oenocytes [33] represent the three major
254 cell types in the fat body. Urocytes store urates either in vacuoles or as circular,
255 birefringent spherocrystals [32], and can occupy a large fraction of the fat body, for
256 instance in the termite *Mastotermes darwiniensis* [32]. In the termite *Reticulitermes*
257 *flavipes*, uric acid is recycled by gut bacteria as a nitrogen source [34], and urate
258 deposits have been linked to oocyte development [35]. In *Pachycondyla* ants,
259 urocytes specialize in the storage of nutrients and excretion products [36] and a
260 composition assay in *Melipona quadrifasciata* bees identified Na, Ca, Mg, P as main
261 elements in urocytes, as well as traces of Zn, Mn, and K [33]. In *C. obscurior* we found
262 circular, birefringent spherocrystals but no cell nuclei, indicating that urate is
263 deposited directly. Worker larvae exhibited small, randomly distributed urate clusters
264 which were found closely associated with what appeared to be trophocytes rather
265 than urocytes. These smaller clusters may originate as a by-product of metabolic
266 processes in trophocytes. Queen larvae showed dense aggregations of urate
267 surrounding the developing ovaries. These large urate deposits may constitute an
268 energy reservoir for cellular growth, a process that is energy-demanding since cells in
269 and around ovaries proliferate at rapid rates.

270 Caste-specific urate patterns only occurred in some *Cardiocondyla* species and in
271 none of the species representing other ant genera. At the moment, we do not know
272 why this is the case. It is unlikely that the presence of the bacterial symbiont *Cand.*
273 Westeberhardia cardiocondylae is directly linked, although in principle it makes for a
274 promising candidate. This endosymbiont with a highly eroded genome resides in

275 bacteriomes associated with the gut and, prominently, with the ovaries in queens,
276 indicating a nutritional link. However, the same urate patterns occur in a *C. obscurior*
277 lineage that is naturally free of *Cand.* Westeberhardia [29], as well as in larvae which
278 have been experimentally cleared of their bacterial symbionts with antibiotic
279 treatment [28]. There is also no obvious phylogenetic signal. *C. obscurior* and its sister
280 species *C. wroughtonii* both exhibit caste-specific patterns but cluster together in
281 clade A with *C. thoracica* and *C. argyrotricha*, both of which do not show the pattern.
282 In clade B, *C. nuda* and *C. venustula,* which exhibit the caste-specific patterns, cluster
283 together with *C. minutior* [15]. A welcome additional coincidence is that all four
284 species with the distinct queen pattern have two alternative male morphs [15] and can
285 be kept in the lab with minimum effort, making the genus perfect for comparative
286 studies of female and male diphenic development.

287 Urate deposit patterns allowed us to reconstruct ovarian development in *C. obscurior*.
288 The female reproductive apparatus is conserved in insects, and consists of two
289 ovaries, the oviduct, the uterus, accessory glands and the spermatheca. Large
290 variation can be found in the number of ovarioles making up each ovary, ranging from
291 1 in a dung beetle, 15-20 in the fruit fly *Drosophila melanogaster* [19], ~200 in honey
292 bees [37] to more than 1000 in some termite and ant species [38]. Six ovarioles in *C.*
293 *obscurior* and *Cardiocondyla nuda* queens [39] mark the lower end in ants, thus
294 allowing detailed study of ovary development in a simple model. In *C. obscurior*, the
295 ovaries develop from a cluster showing early differentiation in L2 larvae to ovaries with
296 differentiated ovarioles in L3 larvae. Nevertheless, the size of urate deposits in L2
297 larvae is similar to that in L3 larvae. Future studies investigating development prior to
298 the L2 stage will reveal when exactly queen and worker phenotypes diverge, and
299 uncover how urate deposits are related to ovary formation.

300 Germline stem cells (GSCs) are typically located in the germarium at the tip of the
301 ovarioles, close to the terminal filament cells ([9,20]. GSCs continuously renew
302 themselves and produce new germ cells. They then proliferate and produce

303 differentiated cystoblasts, which divide synchronously to form cystocytes [21]. These
304 cystocytes are found in the germarium of pupal ovarioles in *C. obscurior,* with some
305 cells larger than others. Cystocystes go on to differentiate into oocytes with their
306 corresponding nurse cells. We suspect that the largest cells are pre-determined
307 oocytes in the pupal germarium, which allow to initiate oocyte maturation soon after
308 hatching. *Cardiocondyla* queens mate inside their natal nest within days of reaching
309 adulthood and can almost immediately begin with the production of offspring [27].

310 The discovery of caste-specific patterns has important implications for understanding
311 both the biology of *C. obscurior* and the general mechanisms underlying caste
312 development in ants. At the life history level, it is now possible to study questions
313 revolving around the phenotypes of developing queens and workers. For example,
314 do the larval phenotypes differ in morphology, behavior or cuticular chemistry? We
315 can also test whether workers discriminate between queen- and worker-destined
316 brood, and if larvae are treated differently depending on caste. In the future, it should
317 even be possible to track individual larvae without the need for tagging by using their
318 unique patterns for individual recognition, similar to the way fins are used to study
319 humpback whales [40]. Creativity limits possibilities now, not vice versa.

320 Because caste-specific urate patterns are already visible in late embryos, we are also
321 finally able to study caste development beyond differentiated features such as wing
322 discs in late larvae [41]. The establishment of *nanos* and *vasa* as reliable expression
323 markers further allows for verification of individual caste identity in molecular studies.
324 *C. obscurior* queens produce increasingly queen-biased caste ratios with age [27],
325 facilitating efficient sampling of queen-destined embryos, and opening numerous
326 avenues for the study of the mechanisms involved in ant caste determination and
327 differentiation, and in social insect polyphenism in general. It has already been shown
328 that ant and honeybee development shares some features, with an overlapping set of
329 genes involved in growth (e.g. TOR, Insulin-like) [42]) and juvenile hormone synthesis
330 and degradation [43] playing a role in developmental regulation [8,30]. Upstream, the

importance of transcription factors involved with the sex differentiation cascade also finds support in ants [17,44], and honeybees [45,46]. Recently, we postulated that a major evolutionary transition, the evolution of sex, has facilitated another major transition, the evolution of eusociality, via co-option of the same developmental switch mechanism [17]. Now we can test this hypothesis, bringing us one step closer to a conceptual understanding of how social insect polyphenism evolved.

Acknowledgements

We thank Alexandra Koch for help rearing embryos, Kristina Pogorelski and Laura Spichtinger for help rearing larvae, Birgit Lautenschläger and Maria Schiwek for help with histology, Erhard Strohm for help identifying the crystalline nature of the deposits, Christopher Winkler for taking pictures, and Lina Pedraza for providing ant species. JO dedicates this paper to Margit Oettler, for nature and nurture. This study was funded by DFG grants (DFG OE549/3-1, OE 549/3-2, OE 549/3-3).

References

1. Boomsma, J. J. & Gawne, R. 2017 Superorganismality and caste differentiation as points of no return: how the major evolutionary transitions were lost in translation. *Biological Reviews* **471**, E1. (doi:10.1111/brv.12330)

2. Light, S. F. 1942 The Determination of the Castes of Social Insects. *The Quarterly Review of Biology* **17**, 312–326. (doi:10.1086/394661)

3. Gößwald, K. & Bier, K. 1954 Untersuchungen zur Kastendetermination in der Gattung Formica. *Insect. Soc.* **1**, 229–246. (doi:10.1007/BF02222948)

4. Brian, M. V. 1973 Caste control through worker attack in the ant Myrmica. *Insect. Soc.* **20**, 87–102. (doi:10.1007/BF02223340)

5. Brian, M. V. 1975 Caste determination through a queen influence on diapause in larvae of the ant *Myrmica rubra*. *Entomologia Experimentalis et Applicata* **18**, 429–442. (doi:10.1111/j.1570-7458.1975.tb00420.x)

6. Trible, W. & Kronauer, D. J. C. 2017 Caste development and evolution in

361 ants: it's all about size. *Journal of Experimental Biology* **220**, 53–62.
362 (doi:10.1242/jeb.145292)

363 7. Abouheif, E. 2021 Ant caste evo-devo: it's not all about size. *Trends in*
364 *Ecology & Evolution* (doi:10.1016/j.tree.2021.04.002)

365 8. Corona, M., Libbrecht, R. & Wheeler, D. E. 2016 Molecular mechanisms
366 of phenotypic plasticity in social insects. *Current Opinion in Insect*
367 *Science* **13**, 55–60. (doi:10.1016/j.cois.2015.12.003)

368 9. Khila, A. & Abouheif, E. 2010 Evaluating the role of reproductive
369 constraints in ant social evolution. *Philosophical Transactions of the Royal*
370 *Society B: Biological Sciences* **365**, 617–630.
371 (doi:10.1098/rstb.2009.0257)

372 10. Schultner, E., Oettler, J. & Helanterä, H. 2017 The role of brood in
373 eusocial hymenoptera. *The Quarterly Review of Biology*, 1–41.

374 11. Pontieri, L., Rajakumar, A., Rafiqi, A. M., Larsen, R. S., Abouheif, E. &
375 Zhang, G. 2020 From egg to adult: a developmental table of the ant
376 Monomorium pharaonis. *bioRxiv*, 2020.12.22.423970.
377 (doi:10.1101/2020.12.22.423970)

378 12. Heinze, J., Cremer, S., Eckl, N. & Schrempf, A. 2006 Stealthy invaders:
379 the biology of *Cardiocondyla* tramp ants. *Insect. Soc.* **53**, 1–7.
380 (doi:10.1007/s00040-005-0847-4)

381 13. Errbii, M., Keilwagen, J., Hoff, K. J., Steffen, R., Altmüller, J., Oettler, J. &
382 Schrader, L. 2021 Transposable elements and introgression introduce
383 genetic variation in the invasive ant Cardiocondyla obscurior. *Molecular*
384 *Ecology* (doi:10.1111/mec.16099)

385 14. Schrempf, A. & Heinze, J. 2006 Proximate mechanisms of male morph
386 determination in the ant *Cardiocondyla obscurior*. *Evol Dev* **8**, 266–272.
387 (doi:10.1111/j.1525-142X.2006.00097.x)

388 15. Oettler, J., Suefuji, M. & Heinze, J. 2010 The evolution of alternative
389 reproductive tactics in male Cardiocondyla ants. *Evolution* **64**, 3310–
390 3317. (doi:10.1111/j.1558-5646.2010.01090.x)

391 16. Cardona, A., Saalfeld, S., Schindelin, J., Arganda-Carreras, I., Preibisch,
392 S., Longair, M., Tomancak, P., Hartenstein, V. & Douglas, R. J. 2012
393 TrakEM2 software for neural circuit reconstruction. *PLoS ONE* **7**, e38011.
394 (doi:10.1371/journal.pone.0038011)

395 17. Klein, A., Schultner, E., Lowak, H., Schrader, L., Heinze, J., Holman, L. &

Oettler, J. 2016 Evolution of social insect polyphenism facilitated by the sex differentiation cascade. *PLoS Genet* **12**, e1005952–e1005952. (doi:10.1371/journal.pgen.1005952)

18. Schmittgen, T. D. & Livak, K. J. 2008 Analyzing real-time PCR data by the comparative CT method. *Nat Protoc* **3**, 1101–1108. (doi:10.1038/nprot.2008.73)

19. Sahut-Barnola, I., Godt, D., Laski, F. A. & Couderc, J.-L. 1995 Drosophila ovary morphogenesis: analysis of terminal filament formation and identification of a gene required for this process. *Dev. Biol.* **170**, 127–135. (doi:10.1006/dbio.1995.1201)

20. Xie, T. 2013 Control of germline stem cell self-renewal and differentiation in the Drosophila ovary: concerted actions of niche signals and intrinsic factors. *Wiley Interdiscip Rev Dev Biol* **2**, 261–273. (doi:10.1002/wdev.60)

21. Okada, Y., Miyazaki, S., Miyakawa, H., Ishikawa, A., Tsuji, K. & Miura, T. 2010 Ovarian development and insulin-signaling pathways during reproductive differentiation in the queenless ponerine ant Diacamma sp. *J. Insect Physiol.* **56**, 288–295. (doi:10.1016/j.jinsphys.2009.10.013)

22. Oettler, J. 2020 *Cardiocondyla*: Heart Node Ants. In *Encyclopedia of Social Insects* (ed C. Starr), pp. 1–4.(doi:doi.org/10.1007/978-3-319-90306-4_19-1)

23. Heinze, J. 2017 Life-history evolution in ants: the case of *Cardiocondyla*. *Proc. Biol. Sci.* **284**, 20161406. (doi:10.1098/rspb.2016.1406)

24. Schrader, L. et al. 2014 Transposable element islands facilitate adaptation to novel environments in an invasive species. *Nature Communications* **5**, 5495. (doi:10.1038/ncomms6495)

25. de Menten, L., Cremer, S., Heinze, J. & Aron, S. 2005 Primary sex ratio adjustment by ant queens in response to local mate competition. *Animal Behaviour* **69**, 1031–1035. (doi:10.1016/j.anbehav.2004.09.005)

26. Oettler, J. & Schrempf, A. 2016 Fitness and aging in Cardiocondyla obscurior ant queens. *Current Opinion in Insect Science* **16**, 58–63. (doi:10.1016/j.cois.2016.05.010)

27. Jaimes Nino, L. M., Heinze, J., Oettler J., 2021 Late-life fitness gains explain the absence of a selection shadow in ants. *bioRxiv* 2021 (doi:https://doi.org/10.1101/2021.02.24.432699)

28. Ün, Ç., Schultner, E., Manzano-Marín, A., Flórez, L. V., Seifert, B., Heinze,

431 J. & Oettler, J. 2021 Cytoplasmic incompatibility between Old and New
432 World populations of a tramp ant. *Evolution* (doi:10.1111/evo.14261)

433 29. Klein, A. et al. 2015 A novel intracellular mutualistic bacterium in the
434 invasive ant *Cardiocondyla obscurior*. *ISME J* **10**, 376–388.
435 (doi:10.1038/ismej.2015.119)

436 30. Schrader, L., Simola, D. F., Heinze, J. & Oettler, J. 2015 Sphingolipids,
437 transcription factors, and conserved toolkit genes: Developmental
438 plasticity in the ant *Cardiocondyla obscurior*. *Molecular Biology and*
439 *Evolution* **32**, 1474–1486. (doi:10.1093/molbev/msv039)

440 31. Schrader, L., Helanterä, H. & Oettler, J. 2017 Accelerated Evolution of
441 Developmentally Biased Genes in the Tetraphenic Ant Cardiocondyla
442 obscurior. *Molecular Biology and Evolution* **34**, 535–544.
443 (doi:10.1093/molbev/msw240)

444 32. Costa-Leonardo, A. M., Laranjo, L. T., Janei, V. & Haifig, I. 2013 The fat
445 body of termites: functions and stored materials. *J. Insect Physiol.* **59**,
446 577–587. (doi:10.1016/j.jinsphys.2013.03.009)

447 33. Furtado, W. C. A., Azevedo, D. O., Martins, G. F., Zanuncio, J. C. &
448 Serrão, J. E. 2013 Histochemistry and ultrastructure of urocytes in the
449 pupae of the stingless bee Melipona quadrifasciata (Hymenoptera:
450 Meliponini). *Microsc Microanal* **19**, 1502–1510.
451 (doi:10.1017/S1431927613013445)

452 34. Potrikus, C. J. & Breznak, J. A. 1981 Gut bacteria recycle uric acid
453 nitrogen in termites: A strategy for nutrient conservation. *Proceedings of*
454 *the National Academy of Sciences* **78**, 4601–4605.
455 (doi:10.1073/pnas.78.7.4601)

456 35. Elliott, K. L. & Stay, B. 2007 Juvenile hormone synthesis as related to egg
457 development in neotenic reproductives of the termite *Reticulitermes*
458 *flavipes*, with observations on urates in the fat body. *Gen Comp*
459 *Endocrinol* **152**, 102–110. (doi:10.1016/j.ygcen.2007.03.003)

460 36. Zara, F. J. & Caetano, F. H. 2004 Ultramorphology and histochemistry of
461 fat body cells from last instar larval of the Pachycondyla (=Neoponera)
462 villosa (Fabricius) (Formicidae: Ponerinae). *Braz J Biol* **64**, 725–735.
463 (doi:10.1590/s1519-69842004000400022)

464 37. Hartfelder, K., Tiberio, G. J., Lago, D. C., Dallacqua, R. P. & Bitondi, M.
465 M. G. 2018 The ovary and its genes—developmental processes
466 underlying the establishment and function of a highly divergent

reproductive system in the female castes of the honey bee, Apis mellifera. *Apidologie* **49**, 49–70. (doi:10.1007/s13592-017-0548-9)

38. Church, S. H., de Medeiros, B. A. S., Donoughe, S., Márquez Reyes, N. L. & Extavour, C. G. 2021 Repeated loss of variation in insect ovary morphology highlights the role of development in life-history evolution. *Proc. Biol. Sci.* **288**, 20210150. (doi:10.1098/rspb.2021.0150)

39. Heinze, J., Kühnholz, S., Schilder, K. & Hölldobler, B. 1993 Behavior of ergatoid males in the ant, Cardiocondyla nuda. *Insect. Soc.* **40**, 273–282. (doi:10.1007/BF01242363)

40. Mizroch, S. A., Beard, J. A. & Lynde, M. 1990 Computer assisted photo-identification of humpback whales. *Rep Int Whale Comm*

41. Oettler, J., Platschek, T., Schmidt, C., Rajakumar, R., Favé, M.-J., Khila, A., Heinze, J. & Abouheif, E. 2019 Interruption points in the wing gene regulatory network underlying wing polyphenism evolved independently in male and female morphs in Cardiocondyla ants. *J. Exp. Zool. (Mol. Dev. Evol.)* **332**, 7–16. (doi:10.1002/jez.b.22834)

42. Mutti, N. S., Dolezal, A. G., Wolschin, F., Mutti, J. S., Gill, K. S. & Amdam, G. V. 2011 IRS and TOR nutrient-signaling pathways act via juvenile hormone to influence honey bee caste fate. *Journal of Experimental Biology* **214**, 3977–3984. (doi:10.1242/jeb.061499)

43. Kayukawa, T., Minakuchi, C. & Namiki, T. 2012 Transcriptional regulation of juvenile hormone-mediated induction of Krüppel homolog 1, a repressor of insect metamorphosis. (doi:10.1073/pnas.1204951109/-/DCSupplemental)

44. Jia, L.-Y., Chen, L., Keller, L., Wang, J., Xiao, J.-H. & Huang, D.-W. 2018 Doublesex Evolution Is Correlated with Social Complexity in Ants. *Genome Biology and Evolution* **10**, 3230–3242. (doi:10.1093/gbe/evy250)

45. Johnson, B. R. & Jasper, W. C. 2016 Complex patterns of differential expression in candidate master regulatory genes for social behavior in honey bees. *Behav Ecol Sociobiol* **70**, 1033–1043. (doi:10.1007/s00265-016-2071-9)

46. Pan, L.-X., Cheng, F.-P. & Wang, Z. L. 2021 Caste-biased Expression of fem and Amdsx Genes in Apis mellifera ligustica (Hymenoptera: Apidae). *Sociobiology* **68**, 5654. (doi:10.13102/sociobiology.v68i2.5654)

503 **Table 1:** Urate deposit patterns predict caste in the ant *Cardiocondyla obscurior*.
504 Survival differences between castes and accuracy of caste prediction were tested
505 using Fisher's exact tests.
506
507

Development stage	Predicted caste	n	Survival			Produced caste		
			Proportion (%)	Differences between castes		Proportion (%)	Accuracy of caste prediction	
				Odds ratio	p		Odds ratio	p
egg	queen	165	24.9 (41/165)	1.276	0.342	78 (32/41)	5.398	<0.001
	worker	192	29.7 (57/192)			42.1 (24/57)		
1st instar larva	queen	34	5.9 (2/34)	1.512	1	0 (0/2)	-	-
	worker	23	8.7 (2/23)			100 (2/2)		
2nd instar larva	queen	50	62 (31/50)	0.334	0.019	90.3 (28/31)	97.129	<0.001
	worker	40	35 (14/40)			92.9 (13/14)		
3rd instar larva	queen	50	60 (30/50)	0.439	0.062	100 (30/30)	infinite	<0.001
	worker	40	42.5 (17/40)			100 (17/17)		

508

509 **Figure legends**

510 Figure 1: Urate deposit patterns distinguish queen- and worker-destined larvae in the
511 ant *Cardiocondyla obscurior*. Stereomicroscope images of worker-destined larval
512 instars (A, C, E) and queen-destined larval instars (B, D, F). Ur = urate.

513 Figure 2: Urate localization in queen- and worker-destined embryos in the ant
514 *Cardiocondyla obscurior*. Worker-destined embryos show no urate (ur) (A), while
515 queen-destined embryos have urate localized in the last segments of their germ band
516 (gb) (B). The first segments of the embryo are clearly separated into the head and the
517 three gnathal segments: mandibular (md), maxillary (mx) and labial (lb).

518 Figure 3: Histological sections of *Cardiocondyla obscurior* larvae. (A) Transversal
519 section of a worker-destined L3 larva. In workers ovaries are missing. (B) Queen-
520 destined larvae show paired ovaries (ov) close to the midgut (mid). (C) In worker-
521 destined larvae urate (ur) accumulates in small randomly distributed deposits. (D)
522 Ovaries in queen-destined larvae are surrounded by large urate deposits. (E) Small

523 urate deposits aggregate close to trophocytes (t). (F) Urate encloses the developing
524 ovary in queen larvae. Tf = terminal filament.

525 Figure 4: Ovarian reconstruction in queens of *Cardiocondyla obscurior*. (A-D) Early
526 gonadal formation in second instar larva. DAPI is used to show the cell nuclei. Vasa
527 stains against germ cells and actin visualizes the cytoskeleton. (A) DAPI staining, (B)
528 Vasa staining, (C) Actin staining, and (D) Merged image with a visible central nervous
529 system (CNS). (E-H) Ovarioles (ov) of a third instar queen larva. (E) DAPI, (F), Vasa, (G)
530 Actin and (H) Merge. The asterisk (*) shows cap cells. (I-L) Ovary of a queen pupa with
531 its six ovarioles. (I) DAPI, (J), Vasa, (K) Actin and (L) Merge. The germ cells have
532 differentiated into cystocytes in this stage, inhabiting the caudal end of the ovariole.
533 Tf = terminal filament. (M-P) Mature ovarioles in adult queens. (M) DAPI, (N) Vasa, (O)
534 Actin and (P) Merge showing the oocyte (oo) with its nurse cells (nc). The oocyte is
535 encircled by follicle cells (fc).

536

537 Supplementary Figure legends

538 Supplementary Figure 1: Dorsal and ventral view of urate patterns in worker- and
539 queen-destined larvae in the ant *C. obscurior*. Stereomicroscope images of worker-
540 destined larval instars (A, C & E) and queen-destined larval instars (B, D & F). (A, B)
541 show larvae in ventral orientation, (C-F) show larvae in ventral orientation. Urate
542 deposits are visible as bilateral symmetrical clusters in queen-destined larvae.

543 Supplementary Figure 2: Types of urate patterns in queen-destined larvae. (A, B) First
544 instar larva with string of pearl-like urate deposits. (C, D) First instar larva with snail
545 shell-like urate deposits.

546 Supplementary Figure 3: Images of queen pupae. (A) Early-stage queen pupa with
547 unpigmented ommatidia and ocelli. (B) Mid stage queen pupa with pigmented
548 ommatidia and ocelli. (C) Example of a 3D rendered ovariole with TrakEM2. Data
549 generated form the reconstruction was used for data analysis. Colors represent

550 individual cells. (D) Cell volume to cell surface in *C. obscurior* queen pupae. The plot
551 illustrates the different sizes of cells in developing cystocytes of queen ovarioles from
552 two pupal stages.

553 Supplementary Figure 4: Caste-specific expression of the germline marker *nanos* in
554 the ant *C. obscurior*. Normalized gene expression of the germline marker in queens
555 and workers in all three larval stages. Expression of *nanos* is significantly higher in L2
556 and L3 queen larvae compared to worker larvae. * $P < 0.05$, Mann-Whitney-U-test.

557 Supplementary Figure 5: Urate patterns distinguish queen and worker-destined larvae
558 in various *Cardiocondyla* species. Stereomicroscope images of queen-destined larval
559 instars (A, B, C) and worker-destined larval instars (D, E, F). (A) Queen larva of *C.*
560 *venustula* (B) Queen larva of *C. wroughtonii*. (C) Queen larva of *C. nuda*. (D) Worker
561 larva of *C. venustula*. (E) Worker larva of *C. wroughtonii*. (F) Worker larva of *C. nuda*.
562 Ur = urate.

563 Supplementary Figure 6: Urate patterns in *Cardiocondyla* species without paired urate
564 deposits. Stereomicroscope images of larval instars. (A) *C. argyrotricha*. (B) *C.*
565 *minutior*. (C) *C. thoracica*. (D) *C. elegans*.

566 Supplementary Figure 7: Urate localization patterns in seven species from four ant
567 subfamilies. Stereomicroscope images of larval instars. (A) *Camponotus mus*
568 (Formicinae). (B) *Formica rufibarbis* (Formicinae). (C) *Linepithema humile*
569 (Dolichoderinae). *Platythyrea punctata* (Ponerinae) (dorsal view). (E) *Wasmannia*
570 *auropunctata* (Myrmicinae). (F) *Temnothorax sp.* (Myrmicinae). Both representatives of
571 the Formicinae are lacking visible urate deposits.

572 Supplementary Figure 8: Schematic illustration of postembryonic ovarian
573 development in the ant *C. obscurior*. The sketched images represent the 2nd instar (A),
574 3rd instar (B) and pupal (C) stage of queens. In the 3rd instar the lateral oviduct (red) is
575 already distinct. The green coloration represents the germ cells as seen in Figure 4.

Figure 1

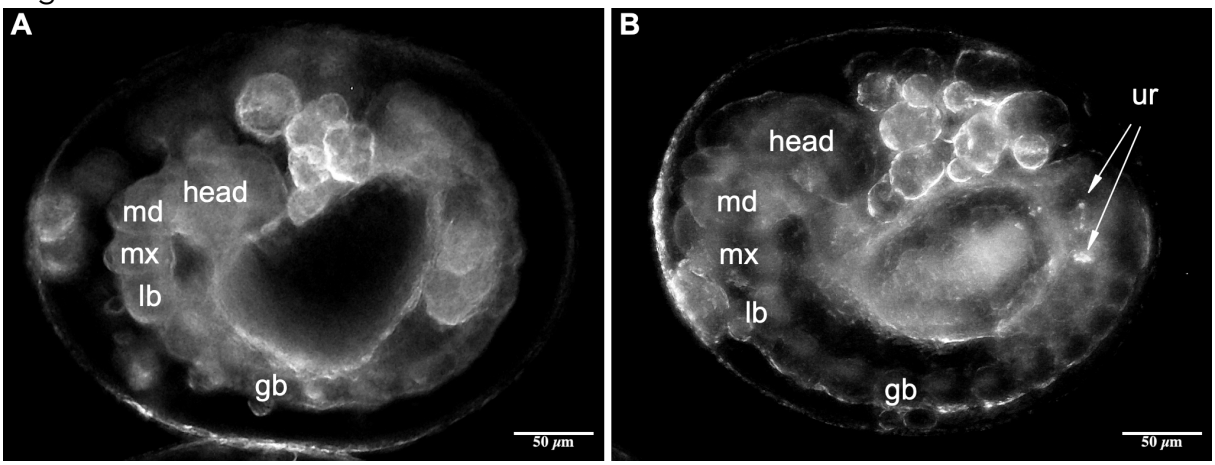

Figure 2

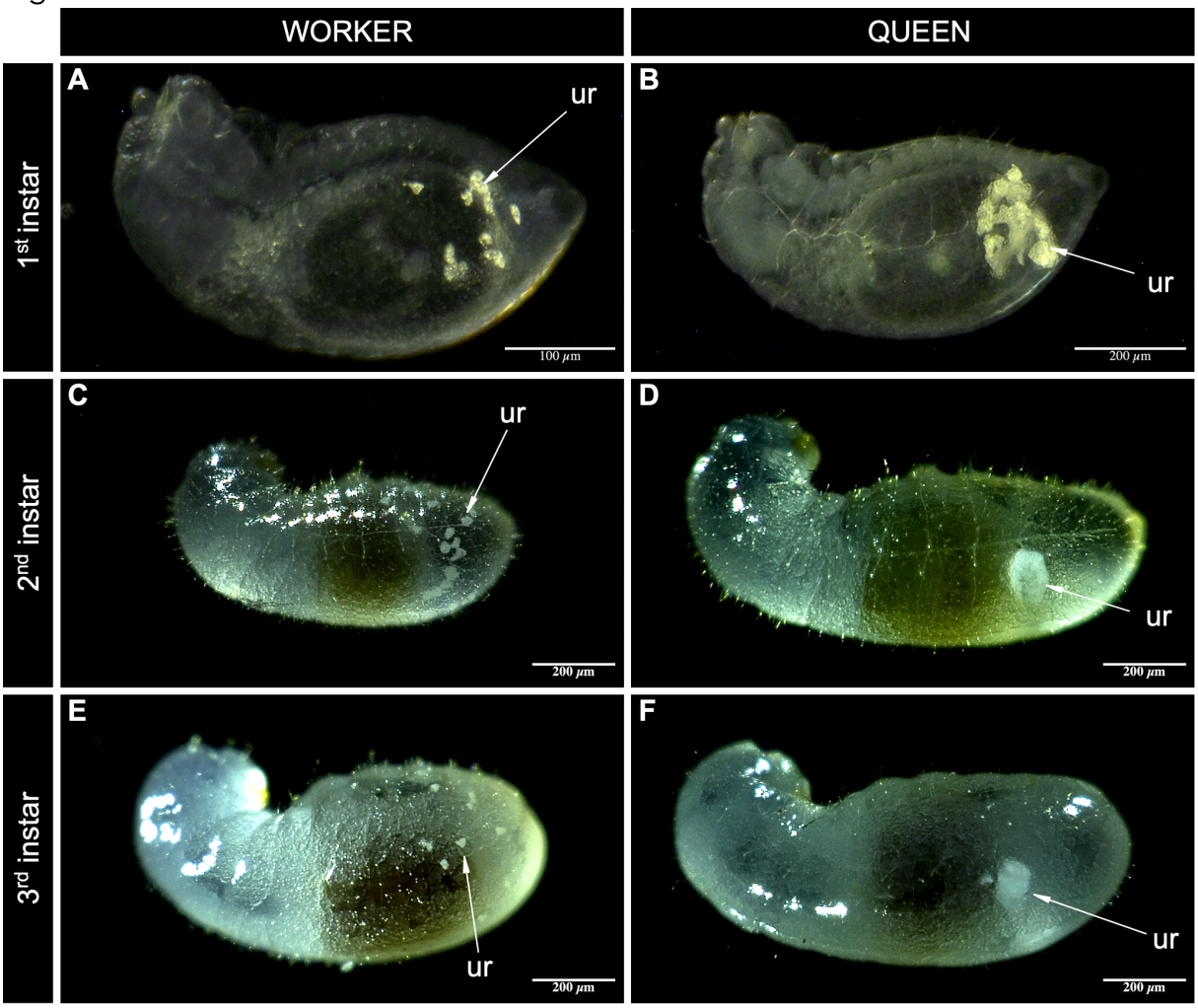
WORKER
QUEEN
1st instar
2nd instar
3rd instar
A
B
C
D
E
F
ur
100 μm
200 μm

Figure 3

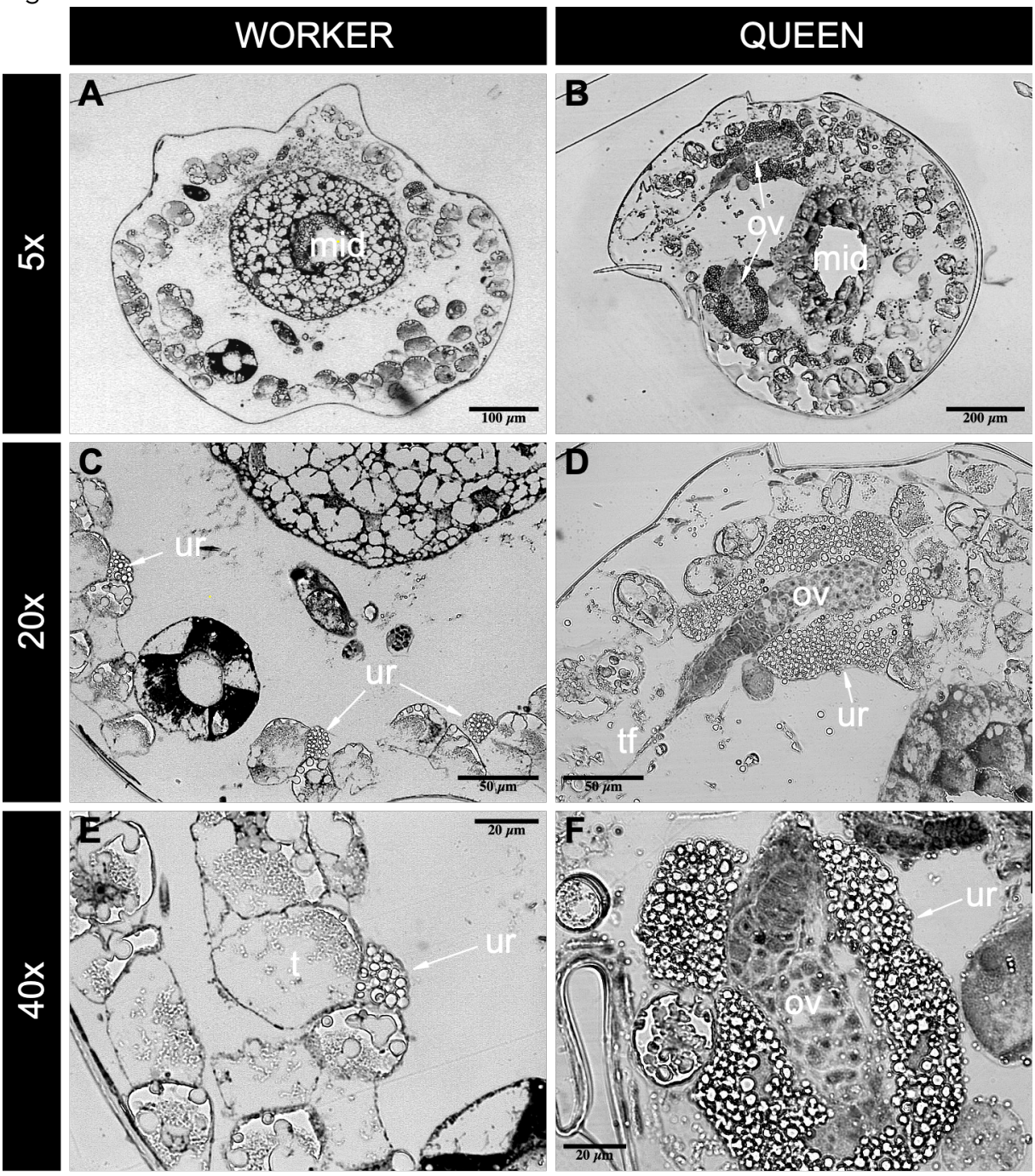
WORKER
QUEEN
5x
20x
40x
A
B
C
D
E
F
mid
ov
mid
ur
ur
ov
ur
tf
t
ur
ur
ov
100 µm
200 µm
50 µm
50 µm
20 µm
20 µm

Figure 4

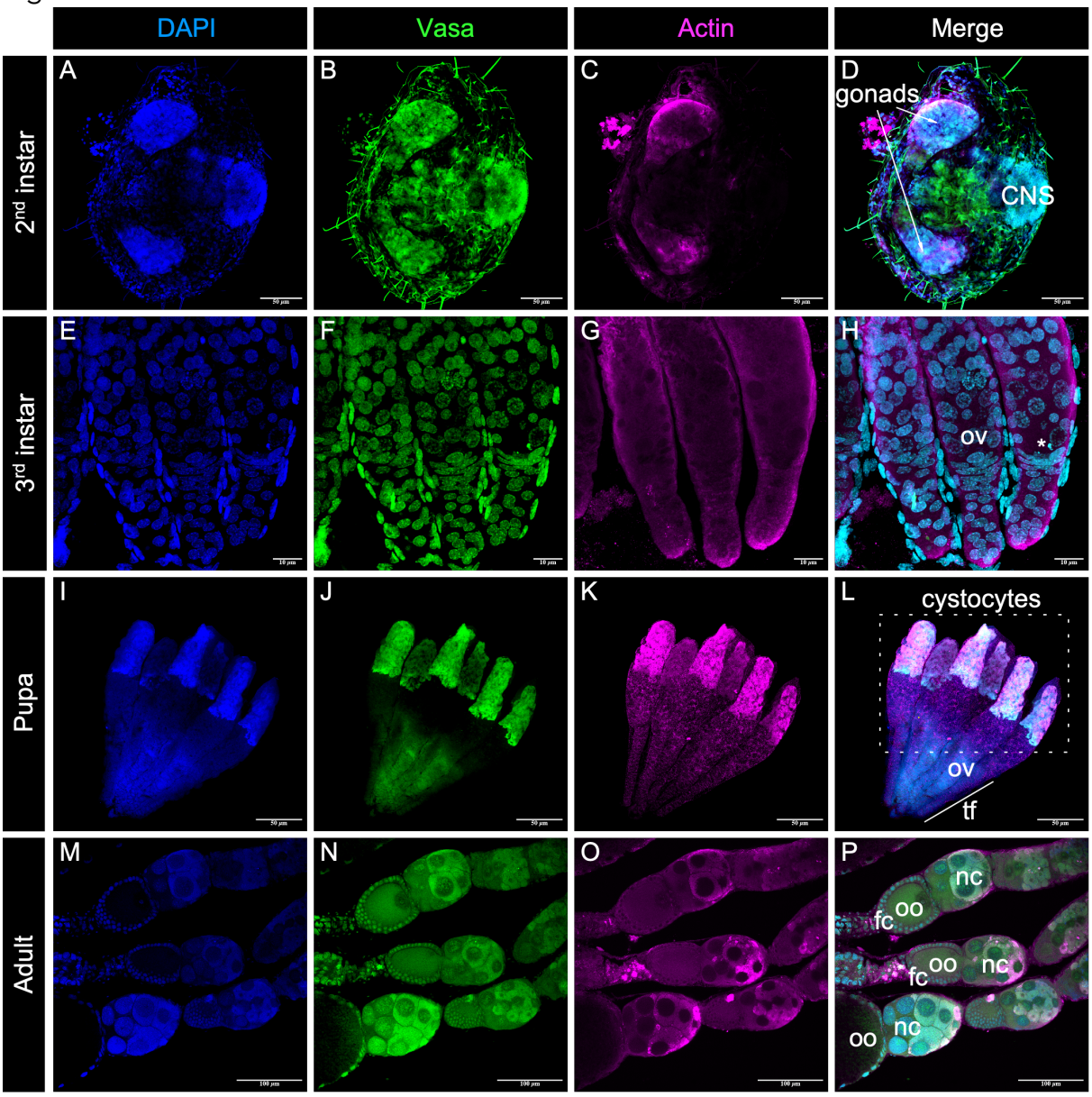
DAPI
Vasa
Actin
Merge
2nd instar
3rd instar
Pupa
Adult
A
B
C
D
gonads
CNS
E
F
G
H
ov
*
I
J
K
L
cystocytes
ov
tf
M
N
O
P
nc
fc
oo
fc
oo
nc
oo
nc